Wideband Modeling of Arbitrarily Shaped H-Plane Waveguide Components by the "Boundary Integral—Resonant Mode Expansion Method"

Giuseppe Conciauro, *Member, IEEE*, Paolo Arcioni, *Member, IEEE*, Marco Bressan, *Member, IEEE*, and Luca Perregrini

Abstract— **The paper describes a very fast and flexible algorithm for the wideband modeling of arbitrarily shaped H-plane waveguide components. The algorithm is based on the evaluation of the poles and the residues of the Y-parameters by the "boundary integral—resonant mode expansion method." It also permits the fast evaluation of the effect of a deformation on the frequency response, a feature very useful either for optimization or for setting the mechanical tolerances. Some examples demonstrate the efficiency, flexibility, and reliability of the method. They show that the frequency response of complicated structures, such as multicavity filters, can be calculated in times of the order of one minute (or less) on ordinary workstations.**

I. Introduction

THE ever-increasing interest in numerical modeling of waveguide components is demonstrated by the huge number of articles and conference papers devoted to this subject in recent years. Some very efficient methods are based on the segmentation of the structure to be analyzed into building blocks represented by generalized circuit matrices or by multimode equivalent circuits [1]–[12]. Anyway, the nature of the analytical/numerical techniques used to model the building blocks (e.g., the mode matching technique) limits the applicability of these methods to structures that can be segmented into elements of very simple shapes. Another approach is based on the field-theoretical analysis of the whole component by general methods, such as the FEM [13], the BEM [14], the FDTD method [15] and the BCMM method [16]. In this approach any limitation on the shape of analyzable components is removed radically, but the resulting algorithms are normally less efficient than the specialized ones, based on the segmentation.

In recent years we developed a field-theoretical method that conjungates the rapidity of specialized methods with the flexibility of general ones. This method is particularly well suited for wideband calculations of irregular responses, due to its nice feature of yielding *in a single step* the mathematical model of a waveguide component in the form of a pole expansion in the frequency domain. In fact, after the model has been identified, the frequency response can be obtained straightforwardly throughout the band of interest, thus avoiding the repeated field calculations that, in other methods, are carried out at many frequency (or time) points. Another relevant feature of our method is the possibility of evaluating very simply the perturbations of the frequency response due to small deformations of the component. This possibility is useful for optimization or for setting machining tolerances.

The method is founded on two cornerstones: i) an approximate—but very accurate—wideband representation of the Y-parameters in the form of a rapidly converging pole expansion; ii) a fast, flexible and reliable algorithm for the calculation of the poles and the residues. This calculation requires the determination of a number of modes of a cavity resonator, i.e., the solution of an electromagnetic eigenvalue problem. The approach to the solution of this problem is based on the same philosophy originally introduced in [17] for the calculation of the modes of hollow conducting waveguides and, more recently, followed in [18], [19] to solve other electromagnetic eigenvalue problems. It is characterized by the use of a hybrid field representation consisting of quasi-static boundary integrals and a rapidly converging resonant mode expansion. For this reason this approach has been recently named "boundary integral—resonant mode expansion (BI-RME) method" [19].

A preliminary paper concerning H-plane structures appeared on a journal of limited circulation [20]. Subsequently, the method has been extended to E-plane and three-dimensional (3-D) structures and, in conjunction with an optimization algorithm, it has been used for the design of components of industrial interest. Short descriptions of these extensions and applications are scattered in a number of conference papers [21]–[27]. Though the details of the theoretical aspects of the method have not yet been described in the literature, the algorithm has already been implemented in a very efficient computer code for the analysis of H- and E-plane waveguide components [28]. The present paper is the first of a series of articles we intend to publish to give a comprehensive description of the BI-RME methodology in the analysis of waveguide components. It is restricted to the H-plane case, which is the simplest one.

Manuscript received July 31, 1995; revised March 20, 1996. This work was supported by MURST.

The authors are with the Department of Electronics, University of Pavia, Via Ferrata 1, I-27100 Pavia, Italy.

Publisher Item Identifier S 0018-9480(96)04706-0.

II. Wideband Representation of the Y-Matrix

Let us consider an arbitrary H-plane component of height h (Fig. 1). The component is lossless and contains a homoge-

neous, isotropic, nondispersive medium whose permittivities are ϵ, μ. We have N terminal waveguides, whose widths (a_n) and lengths (d_n) satisfy

$$d_n \geq a_n \quad (n = 1, 2, \cdots, N). \tag{1}$$

The component is excited by TE_{10}-mode incident waves, at a frequency ω small enough for assuming that, in all waveguides, the evanescent higher order modes generated at the discontinuities are strongly attenuated in the distances d_n. On account of (1) this assumption is acceptable if ω does not exceed some frequency $\omega_{\max}$, about 10% below the cutoff frequency of the TE_{20} mode in the largest waveguide. Up to the frequency $\omega_{\max}$ the component can be described by the admittance matrix $\mathbf{Y} = \mathbf{Y}(\omega)$, that relates the TE_{10}-mode currents and voltages at the ports $S_1, S_2, \cdots, S_N$.

From the theory of cavity resonators we know that the elements of $\mathbf{Y}$ can be represented by the formula [29]

$$Y_{mn}(\omega) = \frac{A_{mn}}{jk\eta} + \frac{jk}{\eta} \sum_i \frac{c_{mi}c_{ni}}{\kappa_i^2 - k^2} \tag{2}$$

where $m, n = 1, 2, \cdots, N$, η is the characteristic impedance of the medium, $k = \omega\sqrt{\epsilon\mu}$ is the wavenumber at the frequency ω and κ_i is the resonating wavenumber of the ith mode of the cavity obtained short-circuiting the ports; furthermore, A_{mn} represents a series depending on the irrational eigenfunctions of the cavity and the coefficients c_{ni} are given by

$$c_{ni} = \int_{S_n} \vec{h}_n \cdot \vec{\mathcal{H}}_i \, dS_n \tag{3}$$

where $\vec{\mathcal{H}}_i$ is the magnetic vector of the ith resonant mode of the cavity and $\vec{h}_n$ is the magnetic vector of the TE_{10} mode of the nth waveguide. Both $\vec{\mathcal{H}}_i$ and $\vec{h}_n$ are normalized to 1 in the cavity volume and in the cross-section S_n, respectively.

Equation (2) is of little practical utility due to the slow convergence of both the modal series and the series represented by A_{mn}. However, we can transform this equation into a more useful one by the following procedure. We have

$$Y_{mn}(\omega) \overset{\omega \to 0}{=} \frac{A_{mn}}{jk\eta} + \frac{jk}{\eta}\left(\sum_i \frac{c_{mi}c_{ni}}{\kappa_i^2} + O(k^2)\right). \tag{4}$$

On the other hand, at low frequencies all waveguides are far below cutoff, so that, provided they are sufficiently long, the ports are practically decoupled and the input admittances are nearly equal to the characteristic admittances Y_n of the TE_{10} mode. Then we can also write

$$\begin{aligned} Y_{mn}(\omega) &\overset{\omega \to 0}{\approx} \delta_{mn} Y_n \\ &= \delta_{mn} \frac{\sqrt{\left(\frac{\pi}{a_n}\right)^2 - k^2}}{jk\eta} \\ &= \frac{1}{jk\eta}\frac{\pi\delta_{mn}}{a_n} + \frac{jk}{\eta}\left[\frac{a_n}{2\pi} + O(k^2)\right]\delta_{mn} \end{aligned}$$

where δ_{mn} is the Kronecker symbol. Comparing with (2) we realize that

$$A_{mn} \approx \frac{\pi\delta_{mn}}{a_n}$$

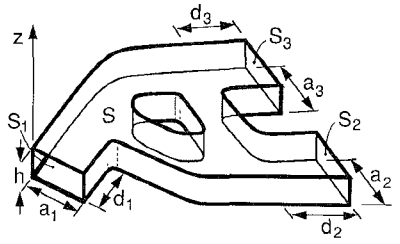

Fig. 1 A H-plane multiport waveguide component

$$\sum_i \frac{c_{mi}c_{ni}}{\kappa_i^2} \approx \frac{a_n\delta_{mn}}{2\pi}. \tag{5}$$

Then, extracting the last series from the series in (2) we obtain

$$Y_{mn}(\omega) \approx \frac{\pi\delta_{mn}}{jk\eta a_n} + \frac{jka_n\delta_{mn}}{2\pi\eta} + \frac{jk^3}{\eta}\sum_i \frac{c_{mi}c_{ni}}{\kappa_i^2(\kappa_i^2 - k^2)}. \tag{6}$$

This equation is much more convenient than (2) due to the improved convergence of the series (caused by the multiplication of its elements by the factor κ_i^{-2}) and because it does not require the knowledge of the irrational eigenfunctions involved in the calculation of A_{mn}.

The systematic error introduced by the approximation (5) decreases with increasing the lengths d_n. To have an idea of its magnitude we considered a waveguide section of length $2d$ and width a, a case where the exact expressions of the resonant wavenumbers κ_i and of the coefficients c_{ni} can be easily determined. Considering a very large number of resonant modes (in order to exclude errors due to the truncation of the series), we calculated the admittance parameters by (6) in the useful band of the waveguide and deduced the return loss, that should be theoretically infinite. We verified an exponential increase, from 32 dB (in the case $d = a$) to 100 dB for $d = 2.5a$. Therefore, under condition (1), the accuracy of (6) is appropriate for most practical purposes.

Using (6) the wideband modeling of a H-plane component is reduced to the problem of determining the first few resonant modes of a cylindrical cavity. The only c_{ni} coefficients that differ from zero are those related to the z-independent TM-to-z resonant modes. These modes depend on a 2-D scalar potential ψ defined in the cross-section S (Figs. 1 and 2) and satisfying the eigenvalue equation

$$\begin{aligned} \nabla^2\psi + \kappa^2\psi &= 0 \quad \text{in } S \\ \psi &= 0 \quad \text{on } \partial S. \end{aligned} \tag{7}$$

Assuming the normalization $\int_S \psi^2 \, dS = 1$, the normalized magnetic field for the ith resonant mode is

$$\vec{\mathcal{H}}_i = \frac{\vec{u}_z \times \nabla\psi_i}{\kappa_i\sqrt{h}}$$

where ψ_i is the ith eigenfunction of (7) and κ_i is the corresponding eigenvalue. Using the well-known expression of $\vec{h}_n$, (3) yields

$$c_{ni} = \frac{1}{\kappa_i}\sqrt{\frac{2}{a_n}}\int_0^{a_n} \frac{\partial\psi_i}{\partial n_n} \sin\frac{\pi\xi_n}{a_n} \, d\xi_n \tag{8}$$

where ξ_n is a coordinate taken over the nth port and $\partial/\partial n_n$ denotes the normal derivative at the same port.

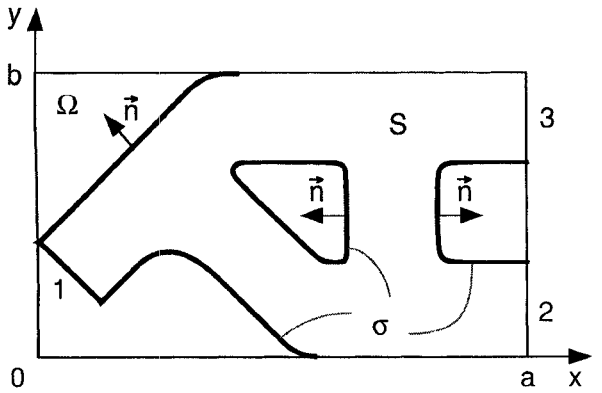

Fig. 2. The cross-section of the short-circuited structure of Fig. 1 embedded in the rectangular domain Ω.

The determination of a sufficient number of eigenvalues of (7) and of the normal derivatives of the corresponding eigenfunctions is all we need to obtain the admittance parameters in the form (6).

III. Determination of the Eigensolutions

The crucial point for setting up an efficient procedure for the determination of the unknown quantities involved in (6) is the choice of the method for finding—with no restriction on the shape of S—a sufficient number of eigensolutions of (7) (in most practical cases this number is of the order of many tens and, sometimes, it can exceed one hundred). General methods, such as the FEM [30], [31] and the BEM [32] are not adequate for finding so large a number of eigensolutions. In fact the use of the FEM would result in a very large matrix eigenvalue problem, and the use of the BEM would require a huge number of repeated calculations of the system matrix, to find the eigenvalues as zeros of its determinant. Therefore, in our application, both methods would result in very long computing times and, in the case of the BEM, in the probable missing of some eigensolutions, especially in regions of closely spaced eigenvalues. The same disadvantages are present in a variant of the BEM proposed in [33], where the usual free-space Green's function is replaced by the Green's function of a fictitious rectangular resonator Ω that includes the domain S (Fig. 2).

Also in our method we consider S as a subdomain of Ω. We extend to Ω the domain of ψ and assume

$$\nabla^2\psi + \kappa^2\psi = 0 \quad \text{in}\,\Omega - \sigma \tag{9}$$

$$\psi = 0 \quad \text{on}\,\partial\Omega\,\text{and}\,\sigma \tag{10}$$

where σ represents the part of ∂S not coincident with $\partial\Omega$. It is evident that, assuming $\psi = 0$ in $\Omega - S$, any eigensolution of (7) is also a solution of the enlarged problem (9), (10). This last problem, however, also admits solutions related to the problem similar to (7) but concerning $\Omega - S$ (or each one of its separate subdomains, as in the case of Fig. 2). These solutions will differ from zero only in $\Omega - S$ (or in one of its subdomains). No solution other than those pertaining to the individual subdomains exists. Note that, in the degenerate cases where the same value of κ is an eigenvalue for two (or more) subdomains of Ω, eigensolutions differing from zero in more than one subdomain may exist. Also in these cases, however, the eigenfunctions can always be combined in such a way as to differ from zero in one subdomain only, like the nondegenerate ones. In conclusion, the solutions of the enlarged problem can be grouped in two classes, "internal" and "external" solutions, differing from zero only in S or in $\Omega - S$, respectively.

Note that all the eigenfunctions of the enlarged problem are continuous in Ω, differentiable to all orders in $\Omega - \sigma$, and with the normal derivative discontinuous through σ. The eigenfunctions, which can be considered real, are orthogonal in the Hilbert space $\mathcal{L}_2(\Omega)$. Since each one of them differs from zero in only one subdomain, normalizing in this subdomain is equivalent to normalizing in Ω. Therefore, in addition to (9), (10) we assume

$$||\psi||_\Omega = 1 \tag{11}$$

where $||\ .\ ||_\Omega$ represents the norm of $\mathcal{L}_2(\Omega)$. The only solutions we are interested in are the internal ones; the external solutions are useless for our purposes. In spite of this, solving the enlarged problem rather than the original one is advantageous due to the possibility of using the BI-RME method, as described in the following subsections.

A. Transformation of the Enlarged Problem into an Integro-Differential Linear Eigenvalue Equation

In the BI-RME method the differential eigenvalue problem is transformed into an integro-differential one, involving new eigenfunctions which are much smoother than the ψ's. The eigenfunctions of the enlarged problem are represented as the sum of: i) a function ϕ, continuous and with continuous normal derivative at σ; ii) another function representing the quasi-static potential produced in Ω by an equivalent source density f located on σ

$$\psi(\vec{r}) = \phi(\vec{r}) + \int_\sigma G(\vec{r},\vec{s})\, f(\vec{s})\, d\sigma \tag{12}$$

where $\vec{r}$ and $\vec{s}$ represent generic positions in Ω and σ, respectively, and G is the Green's function satisfying

$$\nabla^2 G(\vec{r},\vec{r}') = -\delta(\vec{r}-\vec{r}') \quad \vec{r},\vec{r}' \in \Omega$$
$$G(\vec{r},\vec{r}') = 0 \quad \vec{r} \in \partial\Omega. \tag{13}$$

Note that G is known in closed form (involving elliptic functions of a complex variable, see [35], p. 1252) or in the form of a rapidly converging image series (see Appendix A), where the singularity of the Green's function is represented in closed form.

The boundary conditions (10) require

$$\phi = 0 \quad \text{on}\,\partial\Omega$$
$$\phi(\vec{s}') = -\int_\sigma G(\vec{s}',\vec{s}) f(\vec{s})\, d\sigma \quad \forall\,\vec{s}' \in \sigma. \tag{14}$$

Note that, due to the assumed continuity of $\partial\phi/\partial n$, (12) implies that the discontinuity of the normal derivative of ψ resides in the integral, so that, due to a well-known property of the Green's integral, this discontinuity coincides with f. Then, the functional properties of f depend on the behavior

of $\partial\psi/\partial n$ along the boundary; thus we can state that f is continuous and differentiable to all orders along the smooth part of σ, and that the only singularities are possible at the points $\vec{s}^*$ where the direction of the tangent to σ changes abruptly by some angle α. Since the singularities are of the order of $|\vec{s}-\vec{s}^*|^{-\alpha/2\pi}$ and $\alpha<\pi$ (no knife-edge), we can assume that f is square integrable in σ.

Denoting by $\underline{\phi}$ the function ϕ in the subdomain σ and by Lf the boundary integral in (14), we see that f is related to $\underline{\phi}$ by the integral equation

$$Lf=-\underline{\phi}. \tag{15}$$

Note that the domain and the range of the operator L belong to the Hilbert space $\mathcal{L}_2(\sigma)$ because f is square-integrable and $\underline{\phi}$ is a continuous function.

The operator L is positive definite (remember that in electrostatics $\int_\sigma fLf\,d\sigma$ represents the energy of a surface charge of density f). Therefore (15) has a unique solution f for any given $\underline{\phi}$

$$f=-L^{-1}\underline{\phi}. \tag{16}$$

Substituting in (12), we have

$$\psi(\vec{r})=\phi(\vec{r})-\int_\sigma G(\vec{r},\vec{s})\,(L^{-1}\underline{\phi})_{\vec{s}}\,d\sigma. \tag{17}$$

For any ϕ this formula generates a function ψ that satisfies the boundary conditions (10). It is stressed that this formula permits an accurate representation of the discontinuity of $\partial\psi/\partial n$, provided that the singularity of G is expressed in closed form, as we do.

Since the integral in (17) is harmonic in $\Omega-\sigma$, we have

$$\nabla^2\psi=\nabla^2\phi \quad \text{in}\,\Omega-\sigma. \tag{18}$$

Therefore, substituting (18) and (17) in (9), we see that ϕ must be an eigenfunction of the integro-differential linear eigenvalue equation

$$\nabla^2\phi+\kappa^2\left[\phi-\int_\sigma G(\vec{r},\vec{s})\,(L^{-1}\underline{\phi})_{\vec{s}}\,d\sigma\right]=0. \tag{19}$$

Note that the term in parenthesis (that is ψ) is continuous through σ, so that $\nabla^2\phi$ is continuous too. Therefore, i) (19) holds in the whole domain Ω; ii) its eigensolutions are much more regular than those of (9), because their second derivatives are continuous at σ. Each eigensolution of (19) corresponds to an eigensolution of (9) via (17).

Due to (9) and (18), the normalization (11) implies

$$\begin{aligned}1&=\int_\Omega\psi^2\,d\Omega\\&=\kappa^{-4}\int_{\Omega-\sigma}(\nabla^2\psi)^2\,d\Omega\\&=\kappa^{-4}\,\|\nabla^2\phi\|_\Omega^2.\end{aligned}$$

Therefore, ψ is normalized if we enforce on ϕ the condition

$$\|\nabla^2\phi\|_\Omega=\kappa^2. \tag{20}$$

B. Determination of L^{-1}

The inverse of L is determined solving the integral (15) by the Galerkin's method. We consider a set of P basis functions $\{u_p(\vec{s})\}$ belonging to $\mathcal{L}_2(\sigma)$ and approximate f by

$$f=\mathbf{u}^t\mathbf{b}$$

where $\mathbf{u}^t=[u_1,u_2,\cdots,u_P]$ is the row-vector of the basis functions (the superscript t denotes the transpose) and $\mathbf{b}\in\mathcal{R}_P$ is a vector of unknown coefficients. The Galerkin's method converts (15) into the matrix equation

$$\mathbf{L}\mathbf{b}=-\langle\mathbf{u},\phi\rangle_\sigma$$

where $\langle\,\rangle_\sigma$ denotes the inner product of $\mathcal{L}_2(\sigma)$ and $\mathbf{L}$ is the $P\times P$ matrix

$$\mathbf{L}=\langle\mathbf{u},L\mathbf{u}^t\rangle_\sigma. \tag{21}$$

Then we have $\mathbf{b}=-\mathbf{L}^{-1}\langle\mathbf{u},\phi\rangle_\sigma$ and, therefore

$$\begin{aligned}L^{-1}\phi&=-f\\&=\mathbf{u}^t\mathbf{L}^{-1}\langle\mathbf{u},\phi\rangle_\sigma.\end{aligned} \tag{22}$$

The approximations involved in this equation affect the accuracy of the boundary condition $\psi=0$ on σ. Theoretically, increasing the number of basis functions would make the approximation as good as desired; in fact, the positive-definiteness of L assures the convergence of the Galerkin's method [34]. Practically, a wise choice of the basis functions, made in the light of the expected features of f, permits to achieve a very good accuracy with a limited number of basis functions.

C. Determination of the Eigensolutions of (19)

Due to the smoothness of ϕ and $\nabla^2\phi$, we represent these functions by the uniformly convergent Fourier series

$$\begin{aligned}\phi&=\sum_{p,q}a_{pq}\Psi_{pq}\\\nabla^2\phi&=-\sum_{p,q}a_{pq}\lambda_{pq}^2\Psi_{pq}\end{aligned} \tag{23}$$

where the a_{pq} are unknown coefficients and

$$\Psi_{pq}=\frac{2}{\sqrt{ab}}\sin\frac{p\pi x}{a}\sin\frac{q\pi y}{b} \tag{24}$$

$$\lambda_{pq}=\sqrt{\left(\frac{p\pi}{a}\right)^2+\left(\frac{q\pi}{b}\right)^2}\quad p,q=1,2,\cdots. \tag{25}$$

It is noted that the functions Ψ_{pq} are related to the resonant modes of the rectangular box of cross-section Ω in the same way as the eigensolutions of (7) are related to the resonant modes of the short-circuited structure. Then the Ψ_{pq} and the λ_{pq} represent the resonant modes of the rectangular box and their resonant wavenumbers. For this reason, the coefficients a_{pq} will be referred to as "mode amplitudes." The expression obtained by substituting the expansion of ϕ in (17), which consists of a boundary integral and a resonant mode expansion, is the "BI-RME representations" of ψ.

The functions ϕ and $\nabla^2\phi$ are approximated by retaining the first Q modes only in the resonant mode expansions (23).

Due to the smoothness of ϕ, a reasonably small number of the lowest-order modes should be sufficient for an accurate representation of the first eigenfunctions of (19). Therefore we use the approximations

$$\begin{aligned} \phi &= \mathbf{\Psi}^t \mathbf{a} \\ \nabla^2 \phi &= -\mathbf{\Psi}^t \mathbf{\Lambda}^2 \mathbf{a} \end{aligned} \tag{26}$$

where $\mathbf{\Psi}$ and $\mathbf{a}$ are vectors including the retained modes and their amplitudes, respectively, and $\mathbf{\Lambda}$ is the diagonal matrix consisting of the corresponding wavenumbers. With this approximation we also have [see (22)]

$$\begin{aligned} L^{-1}\phi &= -f \\ &= \mathbf{u}^t \mathbf{L}^{-1} \mathbf{R} \mathbf{a} \end{aligned} \tag{27}$$

where $\mathbf{R}$ is the $P \times Q$ matrix

$$\mathbf{R} = \langle \mathbf{u}, \underline{\mathbf{\Psi}}^t \rangle_\sigma \tag{28}$$

(also in this formula the underline indicates $\mathbf{\Psi}$ in the subdomain σ). Due to the orthogonality of the modal fields we have

$$\langle \mathbf{\Psi}, \mathbf{\Psi}^t \rangle_\Omega = \mathbf{I}$$

where $\mathbf{I}$ denotes the $Q \times Q$ unit matrix. Moreover, from the eigenfunction expansion (see [35, p. 821])

$$G(\vec{r}, \vec{r}') = \sum_{p,q} \lambda_{pq}^{-2} \Psi_{pq}(\vec{r}) \Psi_{pq}(\vec{r}')$$

we deduce

$$\langle \Psi_{pq}(\vec{r}), G(\vec{r}, \vec{r}') \rangle_\Omega = \lambda_{pq}^{-2} \Psi_{pq}(\vec{r}').$$

Therefore, introducing (26) and (27) into (19) and using the Galerkin's method (i.e., testing the l.h.s. by $\mathbf{\Psi}$), we obtain the matrix eigenvalue equation

$$(\mathbf{\Lambda}^{-2} - \mathbf{\Lambda}^{-2} \mathbf{R}^t \mathbf{L}^{-1} \mathbf{R} \mathbf{\Lambda}^{-2})(\mathbf{\Lambda}^2 \mathbf{a}) = \kappa^{-2} (\mathbf{\Lambda}^2 \mathbf{a}). \tag{29}$$

Solving this equation we find Q eigenvalues $\{\kappa_1, \cdots, \kappa_Q\}$ and eigenvectors $\{\mathbf{a}_1, \cdots, \mathbf{a}_Q\}$. It is expected that the smallest eigenvalues (that correspond to the most slowly varying eigenfunctions ϕ) are the most accurate approximations for the eigenvalues of (19); in fact (26) approximates ϕ by a band-limited function. so that the approximation is the better the slower the variations of ϕ in comparison with those of the highest order modes included in $\mathbf{\Psi}$. In other words, we expect that the only significant eigensolutions $(\kappa_i, \mathbf{a}_i)$ of (29) are those with κ_i "sufficiently small" in comparison with $\lambda_{\max}$, that is the maximum value λ_{pq} included in $\mathbf{\Lambda}$. For the same reason eigensolutions with $\kappa_i > \lambda_{\max}$ are meaningless, and their calculation can be avoided. Assuming that $(\kappa_i, \mathbf{a}_i)$ is a significant eigensolution of (29), the corresponding eigenfunction is $\phi_i = \mathbf{\Psi}^t \mathbf{a}_i$, and its laplacian is $-\mathbf{\Psi}^t \mathbf{\Lambda}^2 \mathbf{a}_i$. Therefore, it is immediately verified that the normalizing condition (20) requires the following normalization of the eigenvectors

$$\mathbf{a}_i^t \mathbf{\Lambda}^4 \mathbf{a}_i = \kappa_i^4 \tag{30}$$

Due to (17) and (27) the ith normalized eigenfunction of the enlarged problem (9) is given by

$$\psi_i(\vec{r}) = \mathbf{\Psi}^t(\vec{r}) \mathbf{a}_i - \left[\int_\sigma G(\vec{r}, \vec{s})\, \mathbf{u}^t(\vec{s})\, d\sigma \right] \mathbf{L}^{-1} \mathbf{R}\, \mathbf{a}_i. \tag{31}$$

D. Selection of the Internal Modes and Calculation of c_{ni}

Due to the approximation of the method, the internal (external) eigenfunctions cannot be exactly zero in the complementary region. Anyway, each of them can usually be assigned to either region by comparing its magnitude inside and outside S. An exception is expected in cases where some internal and external eigenfunctions are "quasi-degenerate" (i.e., they have very closely spaced eigenvalues); in fact, due to the approximate enforcement of the boundary condition on σ, a sort of "numerical coupling" between the internal and external regions may occur, causing the quasi-degenerate eigenfunctions to differ largely from zero in both regions. In these cases, however, a suitable linear combination of the coupled (or "garbled") eigenfunctions—i.e., a suitable linear transformation of the corresponding eigenvectors—permits us to recover the decoupled ones, that are characterized by largely different magnitudes in the external/internal regions. It is easily shown that, to preserve the normalization (30), the transformation of the eigenvectors must be given by an unitary matrix.

A reliable and easily automatizable procedure for comparing the magnitudes of an eigenfunction in the internal and external regions consists in comparing the norms

$$\begin{aligned} h_i^+ &= \left\| \frac{\partial \psi_i}{\partial n}^+ \right\|_\sigma \\ h_i^- &= \left\| \frac{\partial \psi_i}{\partial n}^- \right\|_\sigma \end{aligned}$$

where the superscripts $+$ and $-$ denote the normal derivatives calculated in the external and internal regions, respectively. These derivatives, deduced from (31), are given by

$$\begin{aligned} \frac{\partial \psi_i(\vec{s}')}{\partial n}^\pm &= \frac{\partial \mathbf{\Psi}^t(\vec{s}')}{\partial n} \mathbf{a}_i - \left[\pm \frac{\mathbf{u}^t(\vec{s}')}{2} \right. \\ &\quad \left. + \int_\sigma \frac{\partial G(\vec{s}', \vec{s})}{\partial n}\, \mathbf{u}^t(\vec{s})\, d\sigma \right] \mathbf{L}^{-1} \mathbf{R} \mathbf{a}_i. \end{aligned} \tag{32}$$

The procedure for selecting the internal eigensolutions and for resolving the garbled ones consists in the following steps:

1) Calculation of h_i^+ and h_i^- for all the eigensolutions with $\kappa_i < \lambda_{\max}$ (as discussed before, all other eigensolutions are meaningless);
2) Sequential testing of the eigensolutions, that are considered internal or external if $h_i^+ < \gamma h_i^-$ or $h_i^- < \gamma h_i^+$, where γ denotes a small number, say 0.05.
3) If a garbled eigensolution ψ_i is encountered, all subsequent garbled eigensolutions ψ_j with $(\kappa_j - \kappa_i)/\kappa_i < \Delta$ (Δ is a small number, say 0.02) are considered as quasi-degenerate with ψ_i. Then each eigenvector $\mathbf{a}_j$ is combined with $\mathbf{a}_i$ in such a way as to minimize or maximize h_i^+. At the end of this process $\mathbf{a}_i$ has been

transformed in such a way as to maximize the unbalance of the magnitudes of ψ_i in the internal/external region. At this point ψ_i is checked again, performing the test described in the previous step.

4) The sequential test is resumed starting from ψ_{i+1}.

The eigensolutions that do not pass the test of step 2 are considered inaccurate. For the reasons discussed before, they are like to occur in the range of eigenvalues nearest to $\lambda_{\max}$. Increasing $\lambda_{\max}$ (i.e., the number of the retained modes) and the number P of the basis functions, the accuracy is increased, and the range of inaccurate eigensolutions can be pushed well above the maximum value of k in the band of interest.

Note that the external derivative $(\partial\psi_i/\partial n)^+$ is nearly zero for the internal solutions. Then, from (32) and (27) we obtain

$$\frac{\partial\psi_i}{\partial n}^- \approx \mathbf{u}^t\mathbf{L}^{-1}\mathbf{R}\mathbf{a}_i = -f_i. \tag{33}$$

This formula can be introduced in (8) for calculating the coefficients c_{ni} pertaining to the ports located on σ. The calculation of the same coefficients pertaining to ports located on $\partial\Omega$ require the numerical evaluation of $\partial\psi_i/\partial n$ on the ports. Since in this case the observation point $\vec{r}$ is outside σ, we have simply

$$\frac{\partial\psi_i(\vec{r})}{\partial n} = \frac{\partial\mathbf{\Psi}^t(\vec{r})}{\partial n}\mathbf{a}_i - \left[\int_\sigma \frac{\partial G(\vec{r},\vec{s})}{\partial n}\mathbf{u}^t(\vec{s})\,d\sigma\right]\mathbf{L}^{-1}\mathbf{R}\mathbf{a}_i. \tag{34}$$

IV. Effect of a Deformation of σ

A deformation of σ causes a change of the frequency response, due to the variation of the resonant wavenumbers κ_i and of the eigenfunctions ψ_i (i.e., of the coefficients c_{ni}). Evaluating the effect of a slight deformation is important both for setting the mechanical tolerances and for including the algorithm in a CAD tool performing the iterative optimization of the response by subsequent deformations of σ.

Let us suppose that a deformation transforms a smooth part of σ by displacing along the normal $\vec{n}$ a generic point from $\vec{s}$ to a new position

$$\vec{s} - \nu\,\Theta\,\vec{n} \tag{35}$$

where ν is a small parameter and $\Theta(\vec{s})$ is a continuous function, differing from zero in the perturbed region only. Furthermore, let us assume to know M resonant modes of the unperturbed structure (i.e., M eigensolutions of (29) related to internal eigenfunctions) and that M is large enough to permit a good accuracy in the calculation of the series in (6). As discussed in Appendix B, the perturbed resonant wavenumbers $(\tilde{\kappa}_1, \cdots, \tilde{\kappa}_M)$ and the perturbed coefficients $\tilde{c}_{n1}, \cdots, \tilde{c}_{nM}$ are given by

$$\tilde{\kappa}_i^2 \approx \kappa_i^2 + \nu\,q_{ii} \tag{36}$$

$$\tilde{c}_{ni} \approx Q_i^{-1/2}\sum_{j=1}^{M}\alpha_{ij}\,c_{nj} \tag{37}$$

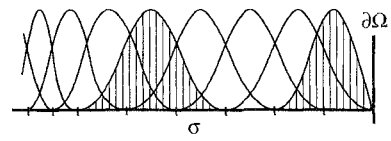

Fig. 3. The piece-wise parabolic splines used as basis functions.

where

$$q_{ij} = \int_\sigma \Theta f_i f_j\,d\sigma \tag{38}$$

$$\alpha_{ii} = \frac{\kappa_i}{\tilde{\kappa}_i} \tag{39}$$

$$\alpha_{ij} = \nu\frac{\tilde{\kappa}_i q_{ij}}{\kappa_j(\tilde{\kappa}_i^2 - \kappa_j^2)} \quad (i \neq j) \tag{40}$$

$$Q_i = \sum_j \alpha_{ij}^2 - \nu\sum_{p,q}\frac{\alpha_{ip}\alpha_{iq}q_{pq}}{\kappa_p\kappa_q}. \tag{41}$$

Using (33) coefficients q_{ij} are given by

$$q_{ij} = \mathbf{a}_i^t\mathbf{R}^t\mathbf{L}^{-1}\mathbf{X}\mathbf{L}^{-1}\mathbf{R}\mathbf{a}_j \tag{42}$$

where

$$\mathbf{X} = \int_\sigma \Theta\mathbf{u}\mathbf{u}^t\,d\sigma.$$

All the matrices in (42) are already known, apart from the perturbation matrix $\mathbf{X}$, whose calculation is straightforward. Then the effect of a deformation can be evaluated with a negligible computational effort. This possibility has actually been exploited for optimization, following a strategy whose description is beyond the scope of the present work.

V. Implementation and Testing of the Algorithm

The boundary σ is approximated by one or more polygonals and the number Q of the modes to be used in the resonant mode expansion is fixed choosing $\lambda_{\max}$ sufficiently larger than the value of k at the upper limit of the operating band of the waveguides. The sides of the polygonal longer than $\pi/2\lambda_{\max}$ are subdivided into segments not exceeding this length.

We use as basis functions piecewise parabolic splines defined over three adjacent segments or—at the extremes of σ—over two segments only (see Fig. 3). A denser segmentation is used near the edges, in order to permit an acceptable approximation of the rapid variations of f. In the calculation of the matrices $\mathbf{L}$ and $\mathbf{R}$, we evaluate all integrals using Gauss quadrature formulas, with the only exception of the entries of $\mathbf{L}$ that involve overlapping basis functions. As usual in the boundary element method, in the calculation of these entries we evaluate the contribution from the singularity of the Green's function analytically, and the contribution from its regular part numerically.

The eigenvalue problem (29) is solved using LAPACK routines.

In the selection of the internal modes the norms h^+ and h^- are calculated in a rather rough (but adequate) manner, by considering the normal derivatives at the midpoint of each segment of σ and summing the products of their squares by the length of the segments. The normal derivative of G is

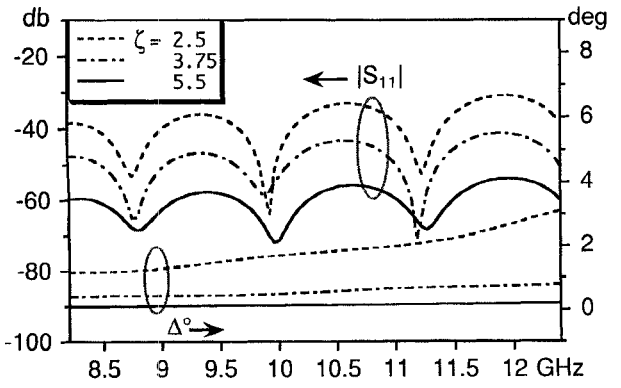

Fig. 4. Effect of the parameter ζ on the magnitude of S_{11} and on the error in the argument of S_{21} for a section of WR-90 waveguide (length = 4 × width). The CPU times were 3 s ($\zeta = 2.5$), 7 s ($\zeta = 3.75$) and 25 s ($\zeta = 5.5$) on a SUN SparcStation 10.

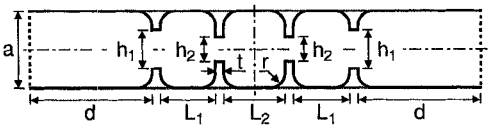

Fig. 5. Geometry of the three-cavity filter. The dimensions (in mm) are: $a = 19.05$; $d = 28.575$; $t = 2.0$; $r = 1.5$; $h_1 = 9.194$; $h_2 = 5.858$; $L_1 = 13.617$; $L_2 = 14.966$.

evaluated using the analytic expression of ∇G deduced from the expression given in Appendix A. The apparent troubles deriving from the numerical evaluation of the principal value integral are absent, because $\partial G/\partial n$ is nonsingular when $\vec{s}$ tends to $\vec{s}'$ in the direction perpendicular to $\vec{n}$.

In the calculation of the coefficients c_{ni} the integrals (8) are evaluated numerically.

After the resonant wavenumbers κ_i and the coefficients c_{ni} have been obtained, the values of the Y-parameters are evaluated at many frequencies in the operating band of the waveguides and the S-parameters are deduced from them.

It is noted that in cases of structures with one or two symmetry planes the algorithm for the mode calculation can be modified to take advantage of symmetry. This modification is not discussed for brevity.

We tested the algorithm using as a benchmark a simple WR-90 waveguide section, whose width is 22.86 mm. In this waveguide the maximum value of k in the band of interest (i.e., at 12.4 GHz) is $k_{\max} = 0.2597$ mm^{-1}. The length of the section was 91.44 mm, i.e., four times the width. As discussed in Section I, with such a length the errors deriving from the approximation in (5) are immaterial, so that the test can give information on the accuracy in the calculations of the eigensolutions and, in particular, on the criterion for the choice of the number of terms to retain in the resonant mode expansion. In the tests the dimensions of Ω were $a = 99.06$ mm and $b = 34.275$ mm.

In the first test we placed the waveguide at the lower left corner of Ω so that σ consisted of two segments, the short one coinciding with a port. The other port was located on $\partial\Omega$. The most critical results to be checked are the magnitude of S_{11} (that should be theoretically zero) and the error $\Delta°$ in the argument of S_{21}. The results of the calculations carried out

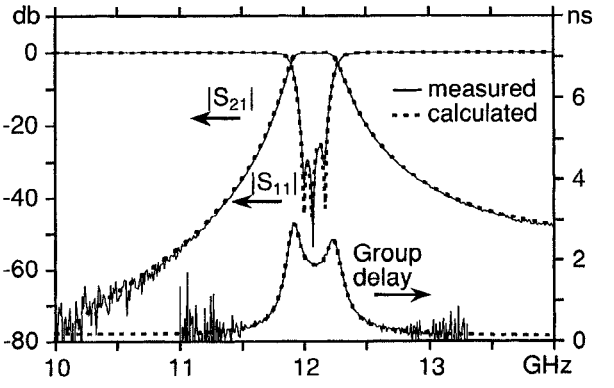

Fig. 6. Calculated and measured response of the filter of Fig. 5. Experimental data, courtesy of ESA-ESTEC (Noordwijk).

with three values of $\zeta = \lambda_{\max}/k_{\max}$ are reported in Fig. 4. It is noted that the accuracy increases with increasing ζ, that demonstrates the convergence of the algorithm. The accuracy is acceptable right from values of ζ as low as 2.5. On the other hand, the CPU time (see caption) increases rapidly with ζ, so that a good trade-off between accuracy and CPU time is to choose ζ in the range $2.5 \div 4$.

In a further test the waveguide was centered in Ω, thus permitting to take advantage of the symmetry. This resulted in a significant reduction of the CPU time, without any significant variation in the accuracy.

VI. Examples

The examples to follow are intended to validate the algorithm and to show how it can be used in the design of complex structures of practical interest, obtaining a very good accuracy with a short computing time (the reported CPU times refer to a SUN SparcStation 10).

The first example concerns the three-cavity filter in WR-75 waveguide, shown in Fig. 5. The measured and the calculated response of the filter are reported in Fig. 6, showing the practical coincidence between them. The experimental data refer to a prototype machined to very close tolerances. In the analysis each rounded corner was approximated by two small segments and the double symmetry was exploited to minimize the computing time. Using $\zeta = 4.5$, the CPU time was only 10 s.

The second example concerns the analysis of the nine-cavity filter shown in Fig. 7, designed using our method in conjunction with an optimization routine. The unusual "meander" shape of this filter was chosen for minimizing its overall length, that is nearly the same as that of a conventional five-resonator in-line filter. Other features of the filter are discussed in [36]. The computed and measured insertion loss of the filter are plotted in Fig. 8. The agreement is very good, in consideration of the fact that the mechanical tolerances were not as good as in the previous example. Using $\zeta = 3.5$, the CPU time was 235 s.

Finally we consider a six-port matched three-way power divider we designed for the $19.7 \div 20.2$ GHz band (see Fig. 9). Ideally, the power entering from any waveguide should be equally divided among the three opposite waveguides, the two

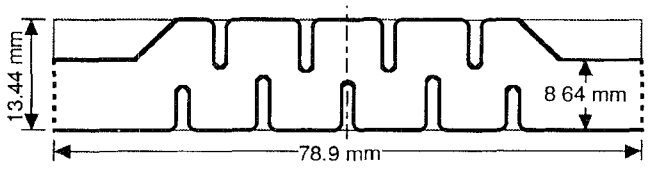

Fig 7. Geometry of the nine-cavity "meander" filter.

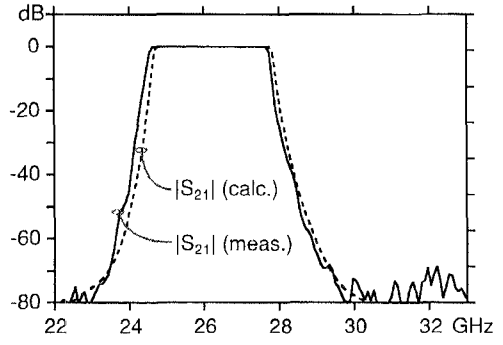

Fig 8. Calculated and measured response of the filter of Fig. 7. Experimental data, courtesy of Siemens TLC (Milano)

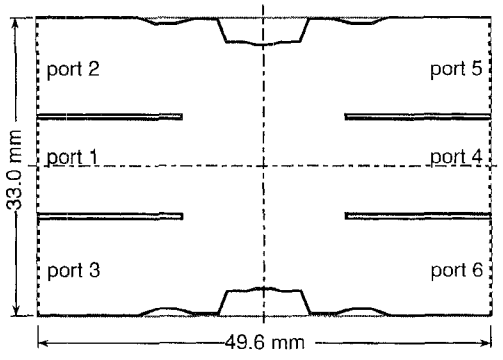

Fig. 9. Three-way matched power divider. The ports are on standard WR-42 waveguides.

port on the same side being decoupled. The complicated shape of the central body of the divider resulted from optimization and derived from the need of minimizing its size (the component was designed for the dividing/recombining network of a spaceborne solid-state power amplifier). The computed and experimental magnitude of some S-parameters are reported in Fig. 10. The agreement is good, the small differences being ascribed partly to mechanical inaccuracies, partly to measuring errors due to the difficulty of connecting the divider to the Network Analyzer. Using $\zeta = 3.5$ the CPU time was 35 s.

VII. Conclusion

We described a method that permits the calculation of all the quantities involved in a mathematical model of H-plane components in the frequency domain. The efficiency of the method depends on the possibility of determining the poles and the residues of the Y-matrix by the solution of a linear matrix eigenvalue problem involving matrices of reasonably small order. The reported examples demonstrate that the wideband modeling of complicate structures, such as multicavity filters of unusual shape, can be carried out in times of the order of one

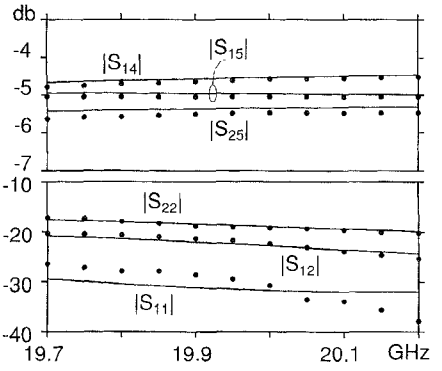

Fig. 10 Computed and measured magnitudes of some S-parameters of the power divider shown in Fig 9. Experimental data, courtesy of Siemens TLC (Milano).

minute, using an ordinary workstation. Either for its rapidity and for the possibility of a quick evaluation of the effect of a deformation on the frequency response, the method is ideally suited for use in a CAD code, together with an optimization routine.

Appendix

A. Expression of G

G can be represented by the image series

$$G(x, y, x', y') = -\frac{1}{2\pi} \sum_{m,\, n=-\infty}^{\infty} (-1)^{m+n} \ln R_{mn}$$

where

$$R_{mn} = [(x - x_m)^2 + (y - y_n)^2]^{1/2}$$

and

$$x_m = \left(m + \frac{1}{2}\right) a + (-1)^m \left(x' - \frac{a}{2}\right)$$

$$y_n = \left(n + \frac{1}{2}\right) b + (-1)^n \left(y' - \frac{b}{2}\right).$$

Summing over n we obtain

$$G = \sum_{m=-\infty}^{\infty} \frac{(-1)^m}{4\pi} \ln \frac{\cosh \dfrac{\pi(x - x_m)}{b} - \cos \dfrac{\pi(y + y')}{b}}{\cosh \dfrac{\pi(x - x_m)}{b} - \cos \dfrac{\pi(y - y')}{b}}.$$

This series converges exponentially. The singularity of the Green's function resides in the term with $m = 0$. If $b > a$ the series summed over m converges more rapidly. This series is obtained by interchanging x with y and a with b.

B. Perturbation Formulas

The perturbation theory reported in [35, pp. 1060–1062] involves the quantities

$$A_{ij} = \int_{\tilde{\sigma}} \frac{\partial \psi_i}{\partial \tilde{n}} \psi_j \, d\tilde{\sigma}$$

$$N_{ij} = \int_{\tilde{S}} \psi_i \psi_j \, d\tilde{S}$$

where ψ_i, and ψ_j are (unperturbed) eigenfunction of (7) and $\tilde{\sigma}$, $\tilde{n}$, and $\tilde{S}$ are the perturbed counterparts of σ, n, and S. Due to the othonormality of the unperturbed eigenfunctions and to the Dirichlet boundary condition we have $N_{ij} \approx \delta_{ij}$, to second order in ν. Moreover, using (7), and writing the first Green's identity for the small region $S - \tilde{S}$, we obtain

$$A_{ij} = -\int_{S-\tilde{S}} \nabla\psi_i \cdot \nabla\psi_j \, d\tilde{S} + \kappa_i^2 (\delta_{ij} - N_{ij}) \approx -\int_{S-\tilde{S}} \nabla\psi_i \cdot \nabla\psi_j \, d\tilde{S}.$$

Therefore, observing that in $S - \tilde{S}$ the normal component of the gradients is nearly constant (within an error of the order of ν^2) and that the tangent component is of the order of ν we have $\nabla\psi_i \cdot \nabla\psi_j \approx (\partial\psi_i/\partial n)(\partial\psi_j/\partial n)$. In conclusion, due to (33) and (35) we can write

$$N_{ij} \approx \delta_{ij}$$
$$A_{ij} \approx -\nu \, q_{ij}$$

where q_{ij} is given by (38). Introducing these expressions in the perturbation formulas (9.2.70) and (9.2.71) reported in [35] we obtain (36) and, for the perturbed eigenfunctions

$$\frac{\nabla\tilde{\psi}_i}{\tilde{\kappa}_i} \approx Q_i^{-\frac{1}{2}} \sum_j \alpha_{ij} \frac{\nabla\psi_j}{\kappa_j} \tag{A1}$$

where α_{ij} is defined by (39), (40) and Q_i is a normalization factor (not considered in [35]). Due to the first Green's identity, the gradients of the eigenfunctions of (7) satisfy

$$\int_S \frac{\nabla\psi_i}{\kappa_i} \cdot \frac{\nabla\psi_j}{\kappa_j} \, dS = \delta_{ij}.$$

Accordingly, Q_i must be determined in such away as to have

$$\frac{1}{\tilde{\kappa}_i^2} \int_{\tilde{S}} \nabla\tilde{\psi}_i \cdot \nabla\tilde{\psi}_i \, d\tilde{S} = 1.$$

Observing that

$$\int_{\tilde{S}} \nabla\psi_i \cdot \nabla\psi_j \, d\tilde{S} = \int_S \nabla\psi_i \cdot \nabla\psi_j \, dS - \int_{S-\tilde{S}} \nabla\psi_i \cdot \nabla\psi_j \, d\tilde{S} = \kappa_i^2 \delta_{ij} - \nu \, q_{ij}$$

we obtain (41). Finally, considering (8), from (A1) we obtain (37).

ACKNOWLEDGMENT

The authors wish to thank Dr. M. Guglielmi of the ESA-ESTEC and Dr. F. Montauti of the Siemens TLC (Milano) for providing the experimental data used to validate the algorithm.

REFERENCES

[1] T. E. Rozzi and W. F. G. Mecklenbrauker, "Wideband network modeling of interacting inductive irises and steps," *IEEE Trans. Microwave Theory Tech.*, vol. MTT-23, pp. 235–245, Feb. 1975.

[2] J. Dittloff, J. Bornemann, and F. Arndt, "Computer aided design of optimum E- and H-plane N-furcated waveguide power dividers," in *Proc. 17th EuMC*, Rome, Sept. 7–11, 1987.

[3] F. Arndt, I. Ahrens, U. Papziner, U. Wiechmann, and R. Wilkeit, "Optimized E-plane T-junction series power dividers," *IEEE Trans. Microwave Theory Tech.*, vol. MTT-35, pp. 1052–1059, Nov. 1987.

[4] J. Dittloff, F. Arndt, and D. Grauerholz, "Optimum design of waveguide E-plane stub-loaded phase shifters," *IEEE Trans. Microwave Theory Tech.*, vol. 36, pp. 582–587, Mar. 1988.

[5] F. Alessandri, G. Bartolucci, and R. Sorrentino, "Admittance matrix formulation of waveguide discontinuity problems: Computer aided design of branch guide directional couplers," *IEEE Trans. Microwave Theory Tech.*, vol. 36, pp. 394–403, Feb. 1988.

[6] M. Guglielmi and C. Newport, "Rigorous multimode equivalent network representation of inductive discontinuities," *IEEE Trans. Microwave Theory Tech.*, vol. 38, pp. 1651–1659, 1990.

[7] J. M. Rebollar, J. Esteban, and J. E. Page, "Fullwave analysis of three and four-port rectangular waveguide junctions," *IEEE Trans. Microwave Theory Tech.*, vol. 42, no. 2, pp. 256–263, 1994.

[8] M. Guglielmi, G. Gheri, M. Calamia, and G. Pelosi, "Rigorous multimode network numerical representation of inductive step," *IEEE Trans. Microwave Theory Tech.*, vol. MTT-42, no. 2 pp. 317–326, Feb. 1994.

[9] A. K. Bhattacharyya, "Multimode moment method formulation for waveguide discontinuities," *IEEE Trans. Microwave Theory Tech.*, vol. 42, no. 8 pp. 1567–1571, Aug. 1994.

[10] F. Alessandri, M. Mongiardo, and R. Sorrentino, "Rigorous mode-matching analysis of mitered E-plane bends in rectangular waveguide," *IEEE Microwave and Guided Wave Lett.*, vol. 4, no. 12, pp. 408–410, Dec. 1994.

[11] R. Beyer and F. Arndt, "Efficient modal analysis of waveguide filters including the orthogonal mode coupling elements by an MM/FE method," *IEEE Microwave and Guided Wave Lett.*, vol. 5, no. 1, pp. 9–11, Jan. 1995.

[12] W. Pascher and R. Pregla, "Analysis of rectangular waveguide junctions by the method of lines," *IEEE Trans. Microwave Theory Tech.*, vol. 43, no. 12, pp. 2649–2653, Dec. 1995.

[13] J. P. Webb, G. L. Maile, and R. L. Ferrari, "Finite-element solution of three-dimensional electromagnetic problems," *IEE Proc, Part H*, vol. 130, no. 2, pp. 153–159, Mar. 1983.

[14] J. Abdulnour and L. Marildon, "Boundary elements and analytic expansions applied to H-plane waveguide junctions," *IEEE Trans. Microwave Theory Tech.*, vol. 42, no. 6, pp. 1038–1045, June 1994.

[15] W. K. Gwarek, "Analysis of arbitrarily-shaped two-dimensional microwave circuits by finite-difference time-domain method," *IEEE Trans. Microwave Theory Tech.*, vol. 36, no. 4, pp. 738–744, Apr. 1988.

[16] J. M. Reiter and F. Arndt, "A boundary contour mode-matching method for the rigorous analysis of cascaded arbitrarily shaped H-plane discontinuities in rectangular waveguides," *IEEE Microwave and Guided Wave Lett.*, vol. 2, no. 10, pp. 403–405, Oct. 1992.

[17] G. Conciauro, M. Bressan, and C. Zuffada, "Waveguide modes via an integral equation leading to a linear matrix eigenvalue problem," *IEEE Trans. Microwave Theory Tech.*, vol. MTT-32, no. 11, pp. 1495–1504, Nov. 1984.

[18] P. Arcioni, M. Bressan, and L. Perregrini, "A new boundary integral approach to the determination of resonant modes of arbitrarily shaped cavities," *IEEE Trans. Microwave Theory Tech.*, vol. 43, no. 8, pp. 1848–1856, Aug. 1995.

[19] M. Bressan, G. Conciauro, and P. Gamba, "Analysis of guided modes in multilayer/multiconductor structures by the boundary integral—Resonant mode expansion method," *IEEE Trans. Microwave Theory Tech.*, vol. 44, no. 5, pp. 659–667, May 1996.

[20] P. Arcioni, M. Bressan, and G. Conciauro, "Wideband analysis of planar waveguide circuits," *Alta Frequenza*, Special Issue Focus on Computer Oriented Design Techniques for Microwave Circuits, vol. LVII, no. 5, pp. 217–226, June 1988.

[21] P. Arcioni and M. Bressan, "Wideband analysis of E-plane waveguide junctions," *Atti della VII Riunione Nazionale di Elettromagnetismo Applicato*, Gruppo di Elettromagnetismo del Consiglio Nazionale delle Ricerche, Frascati, Sept. 5–8, 1988, in Italian.

[22] P. Arcioni and L. Perregrini, "Wide-band optimization of H-plane arbitrarily shaped waveguide junctions," in *Proc. Int. Conf. Electromagnetics in Aerospace Applications*, Torino, Sept. 12–15, 1989.

[23] P. Arcioni, L. Perregrini, and F. Bonecchi, "Low-loss waveguide com-

biners for multidevice power amplifiers," in *Proc. 2nd Int. Conf. on Electromagnetics in Aerospace Applications,* Torino, Sept. 17–20, 1991.
[24] P. Arcioni and L. Perregrini, "Wide-band optimization of E-and H-plane waveguide junctions," in *Proc. IEE Int. Conf. Computation Electromagnetics,* London, Nov. 25–27, 1991.
[25] ——, "Waveguide beam forming network design using a new CAD tool," in *Proc. ESA Advanced Beam Forming Networks Workshop,* Noordwijk, The Netherlands, Nov. 26–28, 1991.
[26] P. Arcioni, M. Bressan, G. Conciauro, and L. Perregrini, "A fast algorithm for the wideband analysis of 3-D waveguide junctions," in *Proc. IEE Second Int. Conf. Computation Electromagnetics,* Nottingham, UK, Apr. 12–14, 1994.
[27] ——, "Fast analysis of waveguide components for antenna feed systems," in *Proc. PIERS 94,* Noordwijk, The Netherlands, July 11–15, 1994.
[28] P. Arcioni, M. Bressan, G. Conciauro, and L. Perregrini, "ANAPLAN-W© on a SUN platform, operating manual," Dip. di Elettronica, Pavia, Final Report, ESA contract no. 10966/94/NL/NB, Mar. 1995.
[29] K. Kurokawa, *An Introduction to the Theory of Microwave Circuits.*New York: Academic Press, 1969, sec. 4.2.
[30] J. B. Davies and C. A. Muilwyck, "Numerical solution of uniform hollow waveguides with boundaries of arbitrary shape," in *Proc. Inst. Electr. Eng.,* vol. 113, pp. 277–284, Feb. 1966.
[31] P. Silvester, "A general high-order finite element waveguide analysis program," *IEEE Trans. Microwave Theory Tech.,* vol. MTT-17, pp. 204–210, Apr. 1969.
[32] B. E. Spielman and R. F. Harrington, "Waveguide of arbitrary cross-section by the solution of a nonlinear eigenvalue equation," *IEEE Trans. Microwave Theory Tech.,* vol. MTT-20, pp. 578–585, Sept. 1972.
[33] Z. Altman, D. Renaud, and H. Baudrand, "Integral equation scalar Green's function formulation for computation of cutoff wavenumbers and modal fields in waveguides," *IEEE Trans. Microwave Theory Tech.,* vol. 42, pp. 532–535, Mar. 1994.
[34] D. G. Dudley, "Mathematical foundations for electromagnetic theory," *IEEE Press Series on Electromagnetic Waves 1994.* New York: IEEE, 1994, p. 35.
[35] P. M. Morse and H. Feshbach, *Methods of Theoretical Physics.* Tokio: McGraw-Hill-Kogakusha, 1953.
[36] M. Guglielmi, F. Montauti, L. Perregrini, and P. Arcioni, "Implementing transmission zeros in inductive-window bandpass filters," *IEEE Trans. Microwave Theory Tech.,* vol. 43, no. 8, pp. 1911–1915, Aug. 1995.

Giuseppe Conciauro, (A'72–M'93) for a photograph and biography, see p. 667 of the May 1996 issue of this TRANSACTIONS.

Paolo Arcioni (M'95) was born in Busto Arsizio, Italy, in 1949. He received the degree in electronic engineering from the University of Pavia, Italy, in 1973.

He joined the Department of Electronics of the University of Pavia as a Researcher in electromagnetics and has taught a course in Microwave Theory as an Associate Professor there since 1976. His current research interest concerns the development of numerical methods for the electromagnetic CAD of passive microwave components. In 1990, he was a Visiting Scientist at the Stanford Linear Accelerator Center, CA, where he was involved with the RF group in the design of optimized cavities for the PEP II project. At present, he cooperates with the National Laboratories of Frascati, Italy, in the design of the accelerating cavities for the DAΦNE storage ring.

Mr. Arcioni is a member of the AEI.

Marco Bressan, (M'93) for a photograph and biography, see p. 666 of the May 1996 issue of this TRANSACTIONS.

Luca Perregrini was born in Sondrio, Italy, in 1964. He received the degree in electronic engineering and the Ph.D. degree from the University of Pavia, in 1989 and 1993, respectively. His Ph.D. thesis dealt with the development of a new algorithm for the analysis of arbitrarily shaped cavity resonators.

In 1992, he joined the Department of Electronics of the University of Pavia as a Researcher in electromagnetics. His current research interests are in the development of numerical methods for the analysis and optimization of waveguide circuits.